Fusion Engineering and Design 218 (2025) 115205

Contents lists available at ScienceDirect

Fusion Engineering and Design

journal homepage: www.elsevier.com/locate/fusengdes

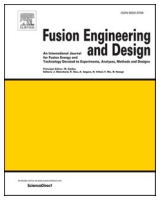

# Design of the WCLL BB in view of the conceptual design phase

P. Arena [a,*], A. Del Nevo [a], J. Aktaa [b], G. Bongiovì [c], L. Bühler [b], I. Catanzaro [c], S. Cesaroni [d], G. Caruso [e], B. Chelihi [f], C. Ciurluini [e], A. Collaku [g], F. Colliva [e], C. Garnier [f], F. Giannetti [e], P. Haghdoust [h], V. Imbriani [i], F. Lucca [h], P. Maccari [a], L. Maqueda [l], L. Melchiorri [e], C. Mistrangelo [b], G. Mongiardini [e], F. Moro [d], T. Moulignier [m], R. Mozzillo [n], S. Noce [d], I. Pagani [h], J.B. Pontier [m], T. Pomella Lobo [b], M. Principato [e], P. Ruiz [l], L. Savoldi [g], S. Siriano [e], A. Tassone [e], F.R. Urgorri [o], F. Viganò [h], Á. Yañez [l]

[a] ENEA, Nuclear Department, C.R. Brasimone, Camugnano, BO, 40032, Italy
[b] Karlsruhe Institute of Technology (KIT), Hermann-von-Helmholtz-Platz 1, Eggenstein-Leopoldshafen, 76344, Germany
[c] Università degli Studi di Palermo, Viale delle Scienze, Edificio 6, Palermo, 90128, Italy
[d] ENEA, Nuclear Department, C.R. Frascati, Frascati, RM, 00044, Italy
[e] DIAEE Department, Sapienza University of Rome, Rome, 00186, Italy
[f] Commissariat à l'Énergie Atomique et aux énergies alternatives (CEA), Saint-Paul-lez-Durance, 13108, France
[g] MATHEP Group, Dipartimento Energia "Galileo Ferraris", Politecnico di Torino, Turin, 10129, Italy
[h] LT Calcoli s.r.l., Via Bergamo 60, Merate, LC, 23807, Italy
[i] CREATE, Department of Industrial Engineering, University of Naples Federico II, Naples, 80125, Italy
[l] ESTEYCO Mechanics, Avenida de Burgos, 12B-Bajo, Madrid, 28036, Spain
[m] Commissariat à l'Énergie Atomique et aux énergies alternatives (CEA), Saclay, 91400, France
[n] CREATE, Engineering Department of Basilicata University, 85100 Campus Macchia Romana (PZ), Italy
[o] CIEMAT, Fusion Technology Division, Avenida Complutense 40, Madrid, 28040, Spain

ARTICLE INFO

*Keywords:*
Fusion
Demo
WCLL
Breeding blanket

ABSTRACT

In view of the definition of the driver blanket for the EU-DEMO fusion reactor, three Breeding Blanket (BB) concepts are being studied in the framework of EUROfusion consortium activities. In mid-2020 two of these concepts, the Water Cooled Lead-Lithium (WCLL) and the Helium Cooled Pebble Bed (HCPB), were reviewed by a panel of external experts to assess the design validity, while the third, the Water-cooled Lead Ceramic Breeder (WLCB), has been recently developed as alternative solution. Thus, starting from the outcomes of the Gate Review, several modifications have been introduced to the WCLL BB design with the aim of addressing the issues revealed by the aforementioned panel.

The present paper reports on main improvements to the WCLL BB design, such as the new water manifold layout to balance the flow distribution among parallel breeding units, the change of the double-walled tube layout to enhance the BB cooling capability and improve its reliability, as well as design solutions aimed at the improvement of the WCLL BB neutronic and structural performances in terms of tritium breeding ratio and verification of design criteria, respectively.

The impact of these changes on nuclear, thermal-hydraulic, MHD and structural performances, as well as on tritium transport, has been evaluated in detail and critically discussed. Finally, the remaining points of improvement are highlighted, giving an overview on possible strategies for their implementation in the WCLL BB design.

## 1. Introduction

The exploitation of nuclear fusion energy for the production of electricity is one of the main challenges of this century [1]. One of the key-points to fulfil this goal is the achievement of a sound and robust design for one of the most important components of each nuclear fusion

* Corresponding author.
*E-mail address:* pietro.arena@enea.it (P. Arena).

https://doi.org/10.1016/j.fusengdes.2025.115205
Received 17 January 2025; Received in revised form 19 March 2025; Accepted 19 May 2025
Available online 24 May 2025

power plant: the Breeding Blanket (BB). This component is therefore in charge of three pivotal functions: collecting the fusion energy arising from the plasma, breeding the tritium for the self-sustainment of the nuclear fusion reactions, as well as shielding the magnets (i.e. toroidal field coils, TFC) and vacuum vessel (VV) from high-energy radiations.

Currently, three BB concepts are being investigated in Europe in the framework of the R&D activities led by the EUROfusion consortium: the Water-Cooled Lead Lithium (WCLL) [2–4], the Helium Cooled Pebble Bed (HCPB) [5,6] and the Water-cooled Lead Ceramic Breeder (WLCB) concepts [7,8]. While the first two concepts have been under development for many years [9], the third concept is relatively recent and is being studied to provide an alternative that addresses inherent risks associated with the HCPB and WCLL concepts.

After the end of the pre-conceptual design phase [9], some design modifications were made to WCLL and HCPB BB concepts to improve their performances and diminish the identified risks. This paper focuses on those relevant to the WCLL BB ones.

As partially reported in [3,4,9], the main issues related with the WCLL BB were a low reliability, as a result of a high number of welds, a small margin against cooling and neutronic performances and low thermal-hydraulic performances in terms of coolant flow distribution. To this purpose, different layouts have been investigated in the last years. One of the main modifications made to the WCLL BB is the adoption of helical Double-Walled Tubes (DWT) in place of the C-shaped ones, as preliminarily investigated and reported in [4,10].

The present paper reports a detailed description of the modifications made to the WCLL BB layout and a comprehensive description of the analysis carried out to evaluate the impact of the aforementioned modifications.

## 2. The WCLL BB layout

The development of the BB in Europe relies since 2018 [2] on some shared cornerstones such as the adoption of the so-called Single Module Segment [11], the adoption of a thick Back Supporting Structure (BSS) to mainly withstand dead and electro-magnetic (EM) loads and housing the attachment with the VV, long poloidal manifold for the distribution and recollection of process fluids and the minimization of feeding pipes. As the WCLL BB envisages two water circuits for the cooling of the structures and liquid PbLi as neutron multiplier, tritium breeder and carrier, a total of six pipes per segment are needed. The only pipes running through the VV lower port are the PbLi inlet ones, while the rest of the pipes are routed through the upper port [4].

Both Inboard and Outboard Blanket (IB and OB, respectively) segments can be thought as a poloidal stack of elementary units, called slices (Fig. 1), which share the same features: a box filled with PbLi and cooled by DWTs in the Breeding Zone (BZ) and by square channels in the plasma facing region, the First Wall (FW). A Back-Plate (BP) delimits the BZ from the region housing PbLi and water manifolds, as well as the BSS.

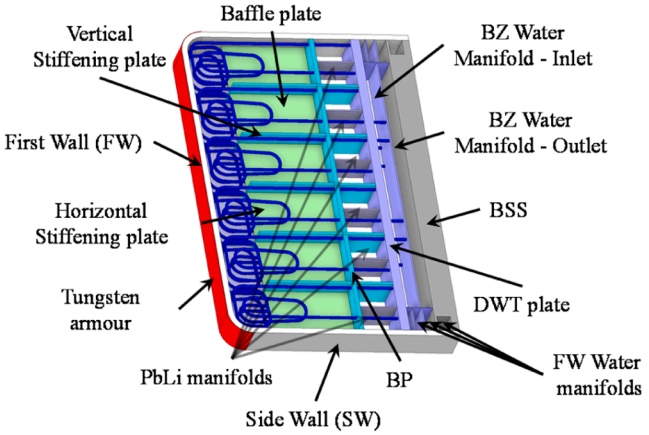


**Fig. 1.** View of the WCLL BZ.

What was deeply changed with respect to the previous WCLL BB configurations is the number and shape of the DWTs, as well as the cooling scheme within the BZ. Indeed, as reported in Fig. 1, the C-shaped DWTs foreseen in [3] have been replaced by helical ones. This design solution should allow designers to achieve, at the same time, different improvements:

- reduction of the number of DWTs (12 per slice in place of 22 or 24 of the previous design) with a significant reduction in the number of welds
- reduction in the water content in the BZ [10], with the goal of increasing the Tritium Breeding Ratio (TBR), trying to reach the target value of 1.15 [12]
- improving the cooling performances of the BZ increasing the margin against the maximum recommended temperature in the structural EUROFER steel of 550 °C
- diminishing the tritium permeation towards the coolant by means of reducing both DWT surfaces wetted by PbLi and breeder average temperature
- improving the mass flow distribution among the different DWTs by removing the recirculation manifold present in the previous configuration

As far as the BZ manifold is concerned, a U-type manifold layout has been adopted in place of the Z-type one [3]. Water entering each segment is split in two streams: about 2/3 of the mass flow is directed toward the bottom part of the segment, whereas the remaining 1/3 feeds the upper part. Moreover, as reported in Fig. 1, inlet and outlet sections of the BZ water manifold have been placed in two different radial levels: the region closer to the PbLi manifold houses the inlet section, the region adjacent to the BSS hosts the outlet one. Thanks to this new configuration, a more balanced mass flow distribution can be achieved. Following sections report in detail the different analyses carried out on the WCLL BB to highlight the impact of the new DWT layout on the BB performances.

Finally, it has to be underlined that the new WCLL BB layout increases the BB representativeness with regards to the ITER WCLL Test Blanket Module (TBM) [13]. This means that results and feedback obtained during the ITER TBM operation could be directly transferred to BB, with a higher return of experience from TBM operation.

## 3. WCLL BB performances

In this section, a detailed overview on the different sets of nuclear, thermal-hydraulic (TH), MHD, structural and tritium transport analysis performed on the new WCLL BB configuration is reported.

### 3.1. Neutronic performances

The neutronic analyses carried out on the WCLL BB are intended to assess its performances in terms of effectiveness in shielding sensitive or structural components of the DEMO reactor (i.e. TFC and VV) as well as to verify its capability to guarantee a suitable Tritium generation rate. Such investigation has been carried out using the MCNP5v1.6 Monte Carlo code [14] complemented with the JEFF 3.3 nuclear data libraries [15].

As for the past studies [16–19], the EU DEMO 1 2017 reference model [20], representing a 11.25° toroidal sector of the machine, has been properly modified to host the MCNP model of the WCLL BB. Taking into account the complexity of the BB structure, the same approach developed in [19] has been employed: it relies on the definition of proper sectors inside the area of the MCNP model dedicated to the BB that will host the main WCLL subcomponents (namely: FW and side walls, BZ, PbLi manifolds and water manifolds). In this way, the

geometry of each subcomponent, defined by means of MCNP 'universes', is independent from the others, thus facilitating the introduction of specific design changes without interfering with the neighbouring elements. The BZ area has been further split into poloidal regions corresponding to the Breeding Units (BUs) foreseen in inboard and outboard (94 and 104, respectively): each of them has been successively filled with the elemental BUs models (Fig. 2) using proper roto-translation matrixes to replicate them along the poloidal direction.

The obtained WCLL DEMO MCNP model, integrating proper material definition according to the specifications [21,22], is shown in Fig. 3.

The MCNP model so far described has been used to assess the following nuclear responses:

- Radial profiles of the neutron flux (total and fast), nuclear heating, He production and damage on stainless steel (SS) components;
- Neutron Wall Loading (NWL) poloidal distribution;
- Total Tritium Breeding Ratio (TBR) considering the contribution of both the BZ and PbLi manifolds.

The neutron source used in the simulations refers to the DEMO conditions, envisaging 1998 MW fusion power plasma scenario with a $7.095 \cdot 10^{20}$ n/s neutron yield.

### 3.1.1. Assessment of the WCLL BB shielding effectiveness

The WCLL BB shielding performances have been evaluated through the analysis of the neutron flux, nuclear heating, damage and He-production in steel components, averaged on a single BU along the inboard and outboard equatorial plane.

The radial profiles of the inboard and outboard total and fast ($E >$ 100 keV) neutron flux are provided in Fig. 4: the neutron flux impinging on the Tungsten FW armour is $4.6 \cdot 10^{14}$ n/cm$^2$/s in the IB segment and $6.2 \cdot 10^{14}$ n/cm$^2$/s in the OB one and it decreases of about three orders of magnitude at the VV outer shell, thus confirming the shielding effectiveness of the BB/manifolds system. The design limit of $10^9$ n/cm$^2$/s for the neutron flux fast component, set to ensure proper functioning of the magnets, is fully satisfied, being $2 \cdot 10^8$ n/cm$^2$/s.

The same trend is highlighted by the analysis of the nuclear heating density radial profiles (Fig. 5) that present a maximum value of 24.5 W/cm$^3$ and 26.9 W/cm$^3$ on the inboard and outboard FW Tungsten armour respectively and scale down to values of the order of $10^{-2}$ W/cm$^3$ on the

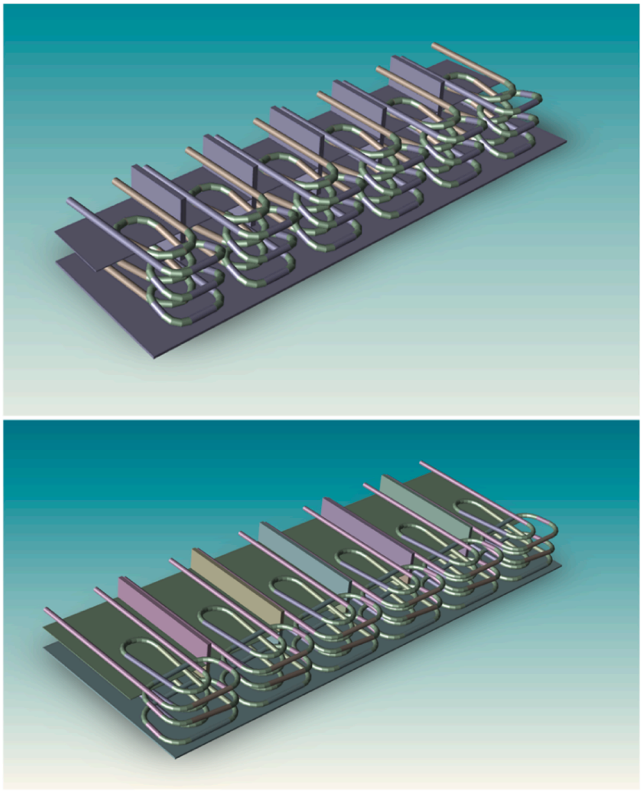

**Fig. 2.** Inboard (upper panel) and outboard (lower panel) BU MCNP models.

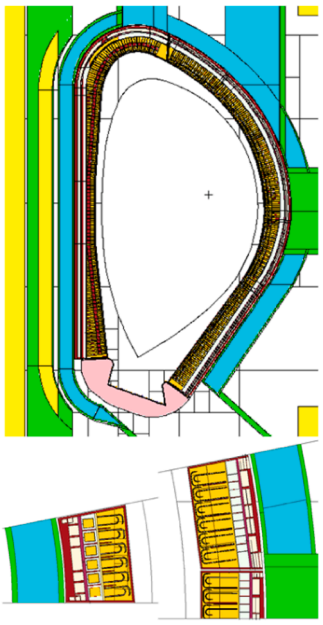

**Fig. 3.** WCLL DEMO MCNP model: poloidal section (upper panel), and toroidal sections along the inboard and outboard midplane (lower panel.).

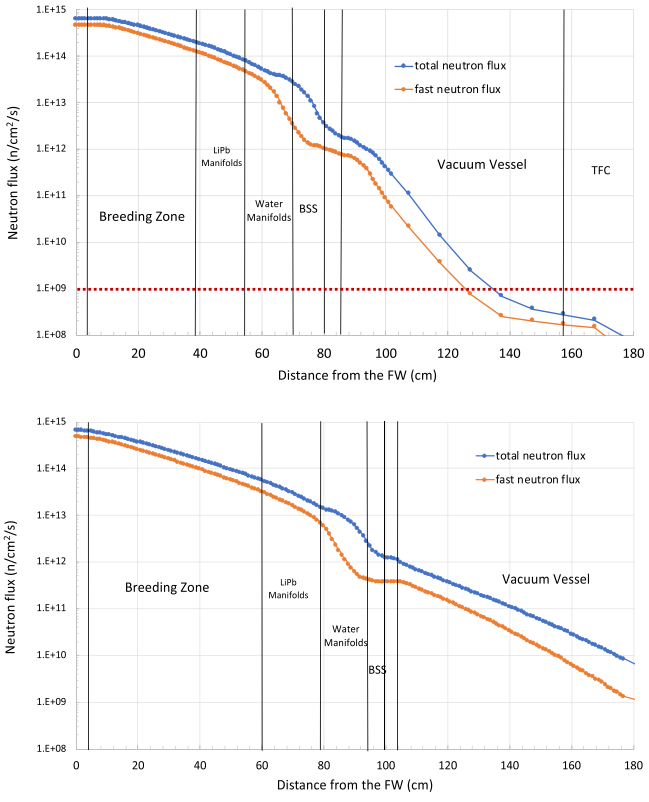


**Fig. 4.** Inboard (upper panel) and outboard (lower panel) total and fast neutron flux radial profiles. The red dotted line refers to the design target for the fast neutron flux on the TFC ($10^9$n/cm$^2$/s).

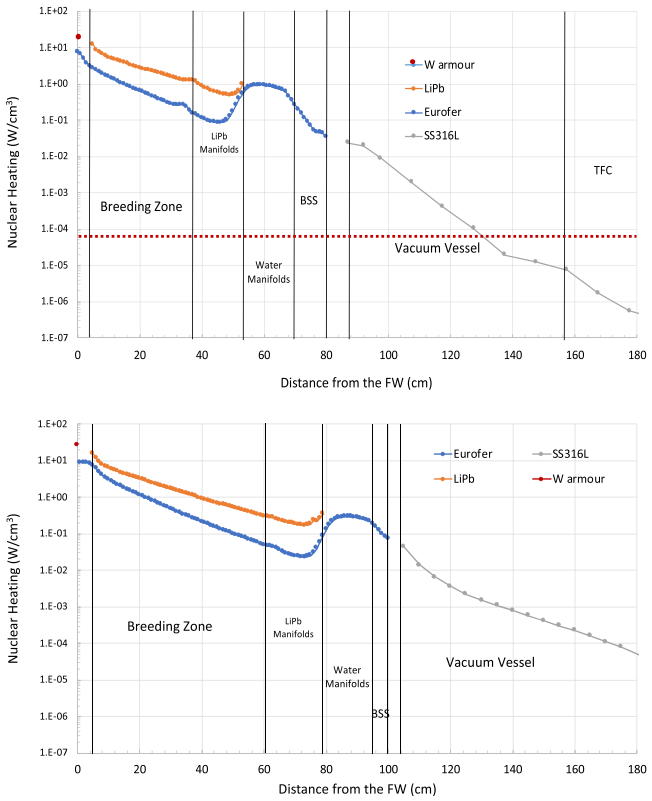


**Fig. 5.** Inboard (upper panel) and outboard (lower panel) nuclear heating density radial profiles. The red dotted line refers to the design target for the heat load on the TFC ($5{\cdot}10^{-5}$ W/cm³).

SS316L VV components. As far as the TFC is concerned, the maximum heat load density is $7.4{\cdot}10^{-6}$ W/cm³, thus the $5{\cdot}10^{-5}$ W/cm³ design limit is satisfied, so a suitable shielding of the magnet system is guaranteed.

The aim of the damage and Helium production assessment is the verification of the structural integrity of the VV and the evaluation of the amount of gaseous products generated in locations where rewelding is foreseen. For the DEMO reactor, the BB must provide enough protection to the VV to ensure a maximum of 2.75 dpa and 1 appm integrated over 6 full power year (FPY) for the damage and the He-production, respectively. The analysis of such nuclear responses on the VV inner shell showed that the damage and the Helium production, cumulated over the DEMO lifetime, are 0.034 dpa and 0.2 appm for the inboard sector and 0.02 dpa and 0.41 appm for the outboard one. In both cases the design limits are fulfilled.

### 3.1.2. *Estimation of the global nuclear parameters: neutron wall loading and total tritium breeding ratio*

The neutron wall loading (NWL) is a fusion power normalised neutron current density impinging on the FW, that enables the design of adequate radial build ups for the BB structure in order to provide suitable shielding against high energy fusion neutrons. Additionally, the evaluation of its poloidal distribution allows a proper scaling of the nuclear heating radial profiles computed at the equatorial level, in order to be used as input for the thermo-mechanical analyses of the other BUs. Fig. 6 shows the NWL poloidal distribution for 1998 MW of fusion power, obtained using as separation surfaces for the tallies the same planes that defined the blanket modules in the previous multi-module-segment configuration [23,24]: the outboard and inboard equatorial zones present the maximum values of 1.33 MW/m² and 1.1 MW/m², respectively, while the poloidal average is 0.93 MW/m²

The analyses performed on the latest WCLL BB design aimed at evaluating its radiation shielding effectiveness, highlighted the

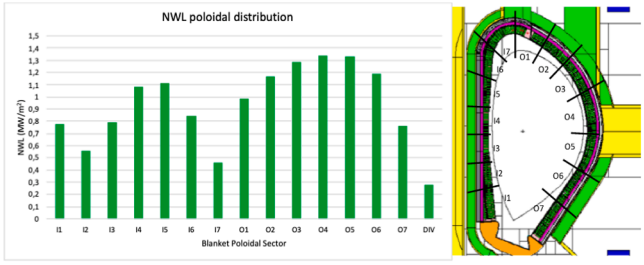


**Fig. 6.** Neutron wall loading poloidal distribution for a 1998 MW fusion power scenario.

beneficial effect of the water in terms of neutron moderation, thus confirming the same behaviour of the previous WCLL architectures [16–19]. However, the WCLL blanket is characterized by reduced Tritium breeding performances with respect to other BB concepts relying on Helium as coolant [25], because of the high amount of water required in the area close to the FW for cooling purposes. As a result, a detrimental impact on the neutron multiplication and, consequently, on the Tritium generation is typically displayed. Despite the reduced overall amount of water with respect to the previous configuration with C-shaped DWTs [10], the total TBR calculated for the present WCLL BB configuration is still below the 1.15 design target for Tritium self-sufficiency [12]. Indeed, when taking into account both the neutron capture reactions on $^{6}$Li and $^{7}$Li isotopes and the contribution from the BZ and the PbLi manifold, the calculated TBR is equal to 1.142.

This outcome triggered a more detailed insight on the underlying physical phenomena behind the Tritium production in the BZ: as a result, a prospective approach relying on an outward radial shift of the DWTs provides promising perspectives to guarantee the Tritium self-sufficiency as well as guidelines for a further improvement of the WCLL BB design [26].

## 3.2. *Thermal-hydraulic performances*

### 3.2.1. *CFD analysis*

A CFD study of the BB cooling performance under steady-state conditions was carried out by considering two slices of the Central OB (COB) segment characterized by different conditions in terms of nuclear heating and heat flux on the FW [27]. The selected slices are those at equatorial elevation (maximum volumetric heat load, minimum surface load) and the pedestrial one, close to the divertor (minimum volumetric heat load, maximum surface load). The volumetric heat load at different poloidal levels is calculated multiplying the nuclear heating distribution calculated at equatorial level for a weighting factor based on the NWL distribution (Fig. 6). The two slices only differ in the number of FW cooling channels, i.e. 4 in the equatorial slice and 6 in the bottom one, as reported in [4]. The different orientation of the FW channels with respect to gravity is not expected to significantly affect the results.

The numerical model of each slice includes the BZ and the FW. The inlet water mass flow rates have been optimized to obtain an averaged outlet temperature of 328 °C with an inlet temperature imposed at 295 °C. The volumetric heating curves (neutrons and γ) were retrieved from the neutronic calculation on the current design (§ 3.1). The main cooling features and boundary conditions adopted in the two calculations (heat

**Table 1**
Values adopted in CFD calculations.

| | Equatorial | Pedestrial |
|---|---|---|
| **FW heat flux [kW/m²]** | 320 [27] | 590 [27] |
| **Nuclear heating [kW/m³]** | from §3.1 | from §3.1 |
| **MFR in BZ [kg/s]** | 1.144 | 0.678 |
| **MFR in FW [kg/s]** | 0.671 | 0.780 |
| **Inlet water T [°C]** | 295 °C | 295 °C |

loads, mass flow rates – MFR, inlet temperatures) are summarized in Table 1. The steady-state CFD simulations of the two models in plasma flat-top conditions were carried out with the Ansys-CFX code. The conservative approximation of solid PbLi was adopted as extensively done in literature.

Results obtained have been compared in terms of temperature field, as reported in Figs. 7 and 8. It can be observed that the temperature of BZ components is much higher in the equatorial slice with respect to the pedestrial one (difference of about 90 °C) because of the higher nuclear heating, while in the FW structure, the temperature difference reduces to about 20 °C. It should be underlined that the maximum recommended value for EUROFER of 550 °C is not reached in both the configurations.

The study carried out provides crucial hints on the BB design for future updates. For instance, it is underlined the need to have a non-uniform distribution of water mass flow rate in BZ at different BB elevations. In particular, a higher BZ mass flow rate is needed in the equatorial region with respect to bottom-elevation region. The water distribution in the FW, on the contrary, might be more uniform at different elevations. Furthermore, the relatively low temperatures obtained in the BZ of the bottom-elevation BUs might suggest a reduction in the number of DWTs to be adopted in this region. An increase of the TBR could benefit from this choice.

A similar study was carried out for a slice placed at the IB segment equatorial level. In this case, the heat flux imposed onto the plasma facing FW is equal to 190 kW/m$^2$ [27], while the nuclear heating is that calculated for the IB segment and reported in Fig. 5. Also in this case results obtained from CFD analyses showed that the new DWT layout is able to extract the nuclear power while maintaining the EUROFER components temperature below the maximum suggested value of 550 °C, as reported in Fig. 9.

### 3.2.2. *Thermal-hydraulic system analyses*

One of the key design issues related to the BB component is the evaluation of its TH behaviour during operational and accidental scenarios. These investigations must be carried out with the aim of identifying potential issues and improving the component layout, as well as considering both local and system scales. The former is fundamental to individuate hot spots where the component can experience undesired and potentially damaging phenomena, such as thermal crisis. The latter is needed to account for the feedback coming from the downwards systems interfaced with the BB, such as the Primary Heat Transfer System (PHTS) and the Power Conversion System (PCS). Within this framework, since 2021, the Nuclear Engineering Research Group (NERG) of Sapienza University of Rome, in collaboration with ENEA, has been developing a System-TH (STH) model of the BB component. The work is in progress, and it is based on a staged approach.

The first step consisted in the preparation of an affordable STH model for the COB equatorial cell to be used for best-estimate calculations [28]. The numerical tool chosen to perform the analyses is RELAP5/Mod3.3 [29], in particular the enhanced version developed throughout the last years at DIAEE, in collaboration with ENEA [30]. The slice design that this work refers to is the WCLL2018.v0.6_B [31,32]. TH simulations were carried by using two DWTs layouts: the old one considering C-shaped tubes and described in [32] and its update with helical-shaped DWTs as discussed in [10]. The RELAP5 model has been developed to evaluate the slice thermal-hydraulic performances in steady state conditions and selected transient load cases. Indeed, the model nodalization comprehends every COB fluid system (PbLi paths, FW cooling tubes, DWTs) and structures. The selected scenarios for this activity were the full plasma power state, pulse-dwell (ramp down) and dwell-pulse (ramp up) transitions and a step-down power transient. Due to the lack of experimental data, STH results were compared to the CFD outcomes, when available. This comparison is fundamental to tune and calibrate the RELAP5 model and to evaluate if the adopted nodalization scheme is able to correctly reproduce the thermal inertia of the COB equatorial cell. This aspect is of primary importance to assess the suitability of the developed input deck and to enhance the reliability of the results obtained with the STH code when simulating the transient scenarios. For what concerns the full plasma power state, the STH model can qualitatively reproduce the CFD outcomes. Some local effects, such as the hot spots in the PbLi thermal field, cannot be represented due to the coarse mesh characterizing the STH approach, see Fig. 10a/d. However, a good agreement was found when the slice average temperatures are compared (between RELAP5 and CFD simulations), and the cell overall thermal inertia is well reproduced. This allows to well reproduce the cell main parameters time trends during the selected operative scenarios (Step-Down, Pulse-Dwell transitions). As an example, Fig. 11 collects the time trends during the dwell-pulse power transition for the DWTs and FW channels inlet/outlet temperatures. A comparison was made between the STH and CFD results. For the DWTs, the C-shaped components are considered because for the new layout the corresponding CFD calculations are still not available. As shown in Fig. 10, the COB transient behaviour predicted by RELAP5 and CFD is almost the same, from both a qualitative and a quantitative point of view.

The second step consists in the development of a STH model of the overall BB sector. The difficulty related to this stage lies in the fact that the cell design varies from one segment to another, and, within each segment, along the poloidal coordinate to accommodate the variations in the power source terms, i.e., heat flux and nuclear heating. It is important to remind that each sector consists of five BB segments and that at each segment correspond nearly one hundred slices piled up in the vertical direction, for a total of five hundred slices per BB sector. Given the limit on the number of components hardcoded in RELAP5 (i.e., 999), it is not possible to simply replicate the STH model developed for the COB equatorial cell for all the cells belonging to a sector. Moreover, this approach would produce an unmanageable input deck and very high time-consuming TH simulations. A better modelling strategy is to group the cells characterized by similar parameters, in terms of boundary conditions (e.g., heat flux, nuclear heating, coolant mass flow, etc.) and/or geometry. For this, the cells in each segment are arranged into 7 poloidal zones. In addition, the two lateral segments (Left and Right ones) in both the IB and the OB were collapsed, since they are identical from the geometrical point of view. As a result, only 21 batches of cells are considered, i.e., seven poloidal zones for three equivalent segment groups. For each batch, the STH model developed for the COB equatorial cell is adopted, with some simplifications, to reduce the number of components adopted. The obtained BB sector model was then used to evaluate its performances during full plasma power state as well as during selected transient scenarios. This work is

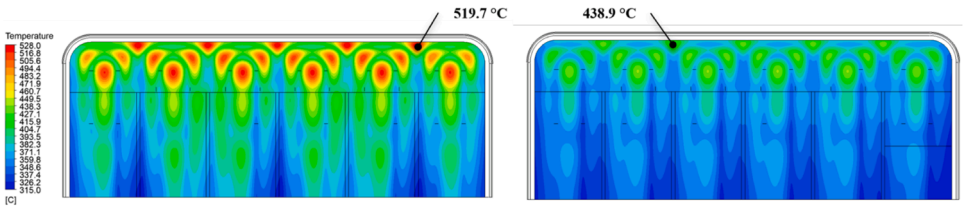


**Fig. 7.** Temperature field on the horizontal plate for equatorial (left) and pedestrial (right) slices.

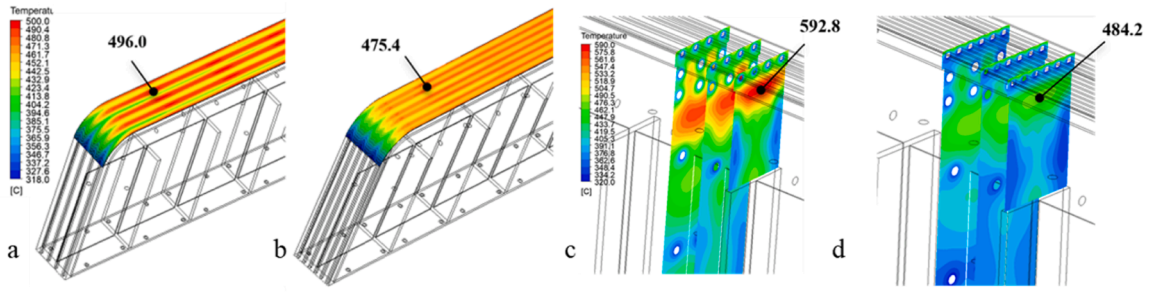


**Fig. 8.** Temperature field in the FW of equatorial and pedestrial slices (a and b, respectively), as well as in the PbLi (c and d).

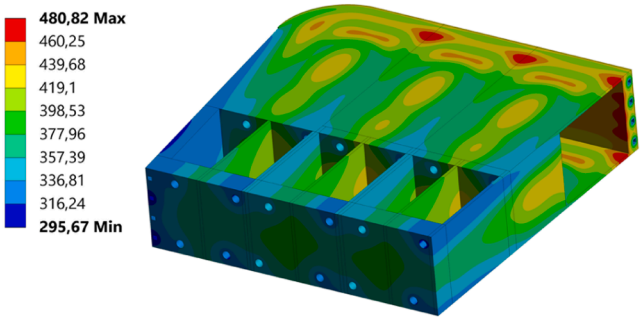


**Fig. 9.** Temperature distribution in the IB equatorial cell.

widely described in [33].

The final goal of this simulation activity is extending the STH model to the overall BB component, considering all the sixteen sectors, and integrating the BB model within a complete Balance of Plant input deck including also the PHTS and PCS. In this way, it is possible to perform a real transient analysis of the EU-DEMO WCLL reactor with the aim of supporting the licensing process.

### *3.2.3. TH analyses of BZ water manifold*

The configuration of the BZ water manifold foreseen in the previous BB design [4,34] was characterised by a significant mass flow unbalance among the different BUs. To this purpose, thanks also to the adoption of the helical DWTs, different manifolds layouts have been investigated. Among them, the U-type manifold connection resulted to be the one with the most uniform mass flow rate distribution, in view of the shaping of the manifolds.

As done in previous studies [3,34], DWTs have been reproduced as Equivalent Porous Pipes (EPPs), with the hydraulic characterizations reported in (1),

$$\Delta P/L = P_{inertial} \cdot v^2 + P_{viscous} \cdot v \quad (1)$$

where $P_{inertial}$ and $P_{viscous}$ are two coefficients accounting for inertial and viscous resistances. These values, reported in Table 2, are calculated from CFD analyses putting in relation pressure drop and mass flow rate values. Due to the toroidal symmetry of the domain (as it can be noted in Fig. 1), only half of the BU has been modelled, so the three couples of DWTs have been modelled as 3 EPPs: EPP1 (the one close to the symmetry plane), EPP2 and EPP3 (the one close to the Side Wall). The total geometry of the COB manifold was addressed, meaning that the flow distribution was computed for all the 104 BUs of the cooling circuit.

The fluid path in the manifolds is shown in Fig. 12. The system is considered adiabatic at the average temperature of 311.5 °C.

The mass flow distribution resulting in the different BUs from the CFD simulation along the entire manifolds is reported in Fig. 13a where it can be appreciated that the first and the second rank of EPPs present a uniform distribution in the bottom and upper branches, but higher mass flow rates are found in the upper one. On the other hand, the third rank of EPPs shows high mass flow rates in correspondence of the inlet at 2/3 the total height of the segment, with a decreasing trend going towards

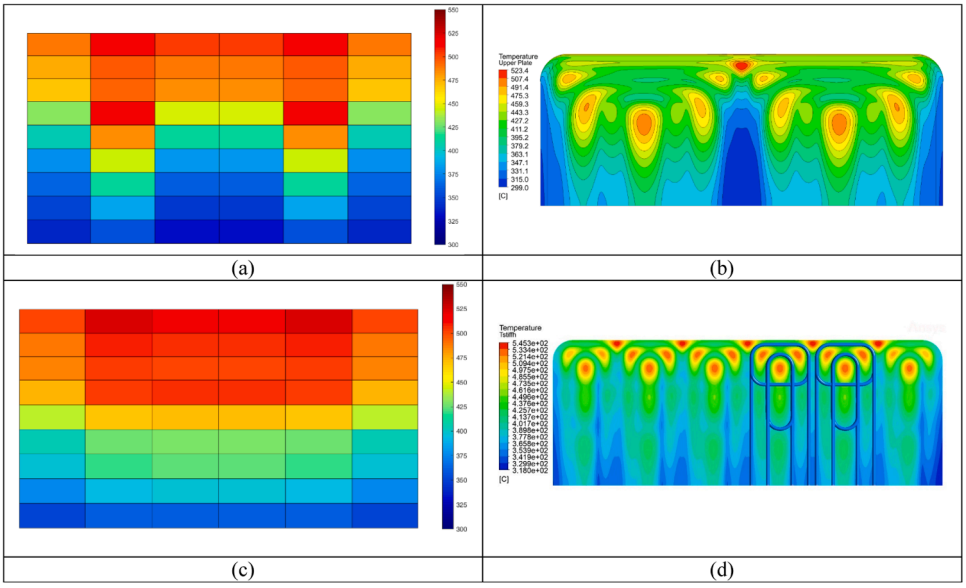


**Fig. 10.** PbLi thermal field within the COB equatorial cell at full plasma power state, comparison between the STH (a and c) and CFD (b and d) outcomes. Both C-shaped (a and b) and helical-shaped (c and d) DWTs layouts are considered.

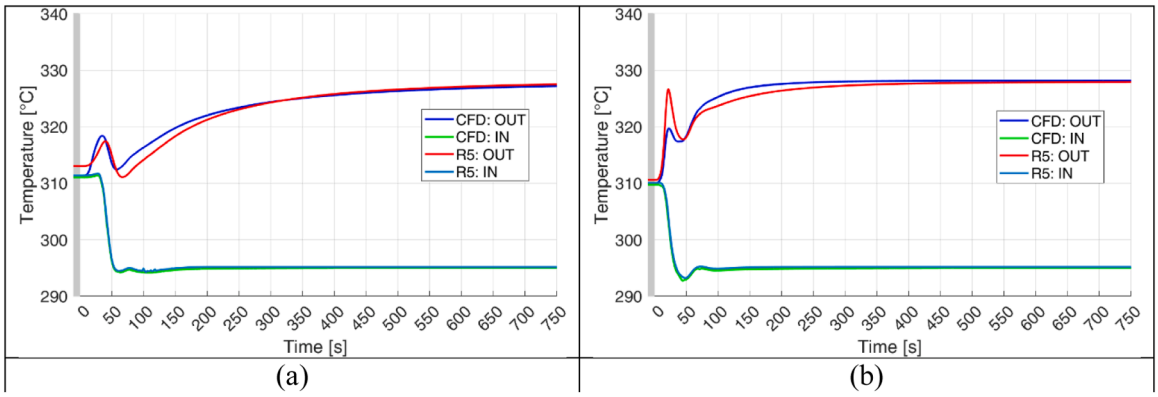


**Fig. 11.** Comparison between STH and CFD results in ramp-up transient load scenario for BZ DWTs (a) and FW channels (b) water. temperatures.

**Table 2**
Inertial and viscous coefficients for the different EPPs.

| | P_inertial [kg•m$^{-4}$•s$^{-2}$] | P_viscous [kg•m$^{-3}$•s$^{-1}$] |
|---|---|---|
| **EPP1** | 5636 | 3599 |
| **EPP2** | 4977 | 3179 |
| **EPP3** | 4954 | 3164 |

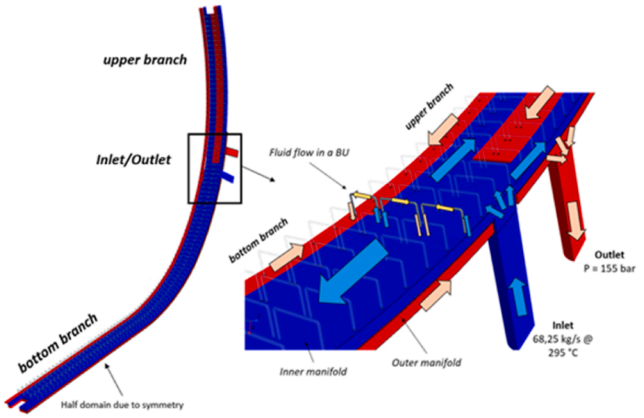


**Fig. 12.** Half of the fluid domain of the total WCLL-BB manifold. Detail of the inlet/outlet region where the two levels of the fluid circuit are visible.

the ends, as expected in a U-type manifold configuration.

Firstly, the imbalance between upper and bottom distributions of the first and second ranks was addressed. The inertial and viscous resistances adopted in the hydraulic characteristics of the EPPs and reported in Equation (1) were calibrated to achieve a uniform distribution between the first two ranks, the result is shown in Fig. 13b. The resistances were calibrated according to Table 3.

The obtained distribution allows to have the first two ranks of cooling tubes, constituting the main heat sink for the blanket, fed with a uniform mass flow rate along the poloidal coordinate. On the other hand, the third rank of cooling tubes gives an additional heat sink contribution in correspondence to the inlet/outlet location (BUs #60 to #80) where higher neutronic loads are expected, resulting in lower mass flow rates in the bottom parts (BUs #1 to #40) where less coolant is needed. Different flow drivers are under investigation, aiming at achieving alternative designs with a uniform flow distribution also along the third rank of EPPs.

### 3.3. Tritium transport performance

The tritium transport analyses aimed at determining the effect of the

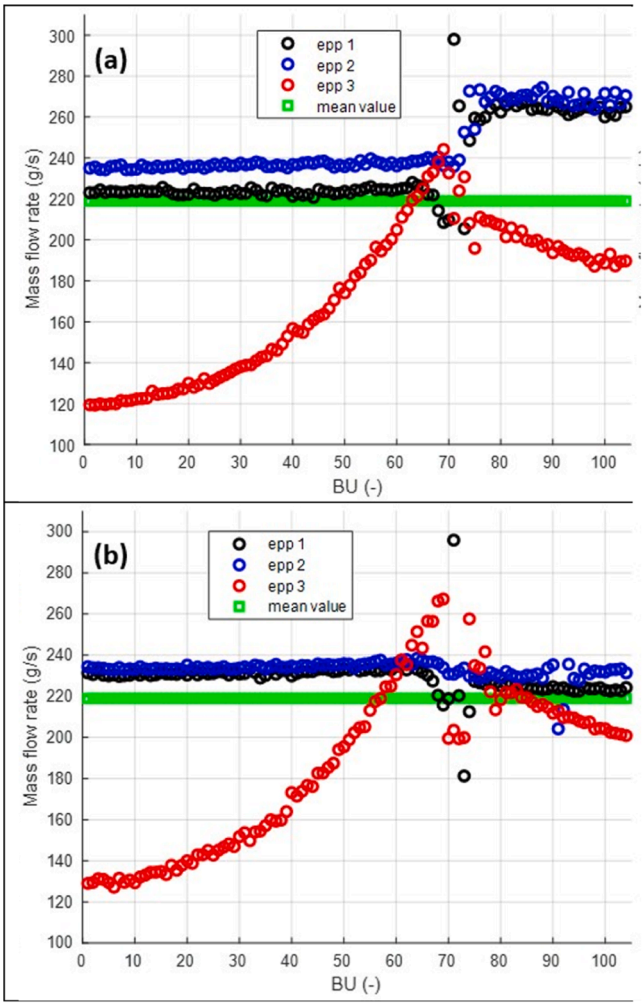


**Fig. 13.** Mass flow rate distribution in the 104 BUs of the cooling circuit of the WCLL BB with the initial configuration (a) and after the hydraulic characteristic calibration (b). BU #1 and #104 refers to the bottom and to the top one respectively. Total inlet and outlet are located in correspondence of BUs #70–75.

helical tube-layout and new manifold arrangement on tritium transport. This design modifications are expected to have a positive effect on reducing tritium permeation rates from breeder to coolant with respect to previous analyses [35,36]. The main reasons are the reduction on the contact surface between the PbLi and DWTs and the colder PbLi

**Table 3**
Percentage of increment of the inertial and viscous resistances in the bottom and upper branches of the manifold for rank #1 and #2.

| | | P_inertial | P_viscous |
|---|---|---|---|
| **EPP1** | **Bottom** | +20 % | +20 % |
| | **Up** | +80 % | +80 % |
| **EPP2** | **Bottom** | +30 % | +30 % |
| | **Up** | +80 % | +80 % |

temperature map (in particular close to the FW) with respect to the previous C-shaped tube configuration.

The model has been developed using the tritium transport libraries of EcosimPro. This code models 1D transport equations in the solid and fluid domains using a finite volume approach. The 1D components are connected following a process flow diagram whose objective is representing the major tritium transport pathways in the blanket geometry. The procedure is based on implementing a detailed model of the equatorial COB slice and then scaling the results using the breeder volume to obtain global blanket outcomes. This strategy has been implemented and described in detail in the past for other designs [37,38]. The global input parameters are depicted in Table 4. To be noted that, even though the nominal Coolant Purification System (CPS) extraction efficiency is 90 %, only a small portion of the water flow rate can be processed, so its effective efficiency is greatly limited.

It is important noting that, following the reference permeation reduction strategy, the cooled PbLi-steel interfaces feature a permeation barrier that are modelled by applying a permeation reduction factor (PRF). The macroscopical properties of the PbLi are taken from Reiter [39] while the EUROFER properties are taken from the works of Esteban et al. [40] and Peñalva et al. [41]. Finally, the three-trap model of Montupet-Leblond et al. [42] has been implemented for EUROFER.

The most important model outcomes are shown in Table 5, after 2 full-power years (fpy). Permeation rates inside the blanket oscillate around a steady-state value due to the generation pulses considered for DEMO (Fig. 14). The total permeation rate from PbLi to water is reduced by approximately a factor 2 with respect to the previous tube configuration.

As mentioned, the model computes tritium transport inside the COB equatorial slice with more detail. Therefore, using the global signals of the system, the model is able to compute 1D local concentrations distributions in the PbLi circuit as shown in Fig. 16. The obtained tritium exit concentration in the breeder is equal to $8{\cdot}10^{-3}$ mol/m$^3$.

Considering the tritium losses, the most important contribution is the permeation from the PbLi pipes to the room (PHTS area). Fig. 15 depicts this permeation rate. The step-like shape of the curve is caused by the saturation of the two high energy traps of EUROFER. It is important to remark that in the PbLi pipes no permeation barriers are imposed. The second contribution to the tritium losses is the permeation from primary to secondary circuits in the steam generators and heat exchangers of the system. However, this contribution is several orders of magnitude smaller.

The two intrinsic (i.e. not irradiated) high energy traps reported by Montupet-Leblond et al. in EUROFER produce trapped inventories of the order of 100 g (see Fig. 17). The higher contribution, about 135 g, is located in the manifolds where there are large volumes of steel at relatively low temperatures. Lower values are calculated for the BZ (~90 g) and PbLi loop (40 g). Besides, transient times are greatly increased as the trapping-detrapping equilibrium needs long times to be reached everywhere (from ~1–10 days without traps to ~200 days). This is the first time that a multi-trapping model of such characteristics is applied to a global systems-level model.

**Table 4**
Global input parameters of system level tritium transport model.

| | |
|---|---|
| Blanket tritium generation rate [g/day] | 320.26 |
| In-vessel PbLi volume [m$^3$] | 878.56 |
| Ex-vessel PbLi volume [m$^3$] | 80.7 |
| Total PbLi mass flow rate [kg/s] | 1625 |
| In-vessel water volume [m$^3$] | 195.31 |
| Ex-vessel water volume [m$^3$] | 324.29 |
| Total water mass flow rate [kg/s] | 9936 |
| Permeation surface in an OB slice [m$^2$] | 1.4 |
| PRF in wetted surfaces [-] | 100 |
| TES extraction efficiency [ %] | 80 |
| CPS effective extraction efficiency [ %] | $6.58{\cdot}10^{-5}$ |

**Table 5**
Results of tritium transport analyses after 2 fpy.

| | |
|---|---|
| Permeation rate from PbLi to BZ circuit [mg/day] | 65.85 |
| Permeation rate from PbLi to FZ circuit [mg/day] | 17.16 |
| Permeation rate from PbLi to PHTS area [mg/day] | 26.81 |
| Permeation rate to the secondary fluids [mg/day] | 0.045[1] |
| Tritium inventory in PbLi (in-vessel) [g] | 14.13 |
| Tritium inventory in water (in-vessel) [g] | 15.49 |
| Tritium mobile inventory in EUROFER (in-vessel) [g] | 2.82 |
| Tritium trapped inventory in EUROFER (in-vessel) [g] | 225.64 |
| Tritium inventory in PbLi (ex-vessel) [g] | 0.49 |
| Tritium inventory in water (ex-vessel) [g] | 16.48 |
| Tritium mobile inventory in EUROFER (ex-vessel) [g] | 0.13 |
| Tritium trapped inventory in EUROFER (ex-vessel) [g] | 40.79 |

[1] The steady-state value is not reached after 2 fpy for this signal.

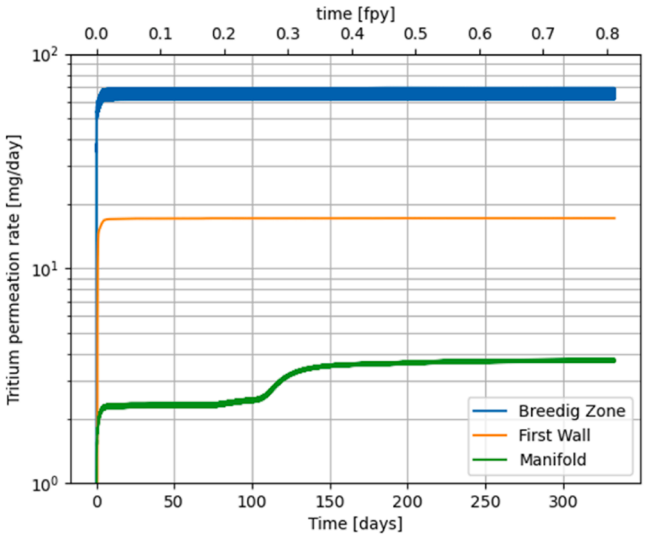


**Fig. 14.** Tritium permeation rates inside the blanket from PbLi to water.

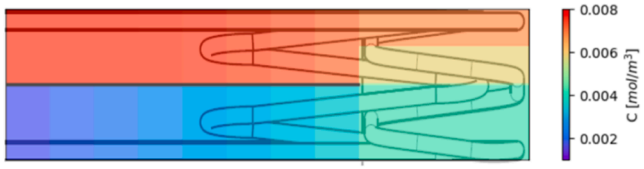


**Fig. 15.** Steady-state tritium concentration inside PbLi.

### 3.4. MHD performances

Magneto-hydro-dynamic (MHD) activities carried out to support the WCLL BB design are mainly divided into two main branches. The first deals with the detailed magneto-convective assessment of the BZ region enclosed between the baffle plate and the FW. The second concerns the analysis of the PbLi manifold behaviour and the distribution of the PbLi between the different slices (also called breeding units - BU) fed in parallel by this component.

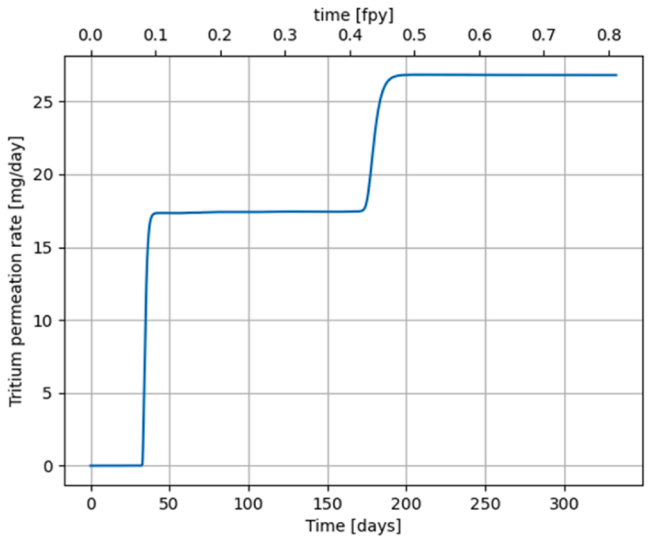


**Fig. 16.** Tritium permeation rate from the TER to the PHTS area.

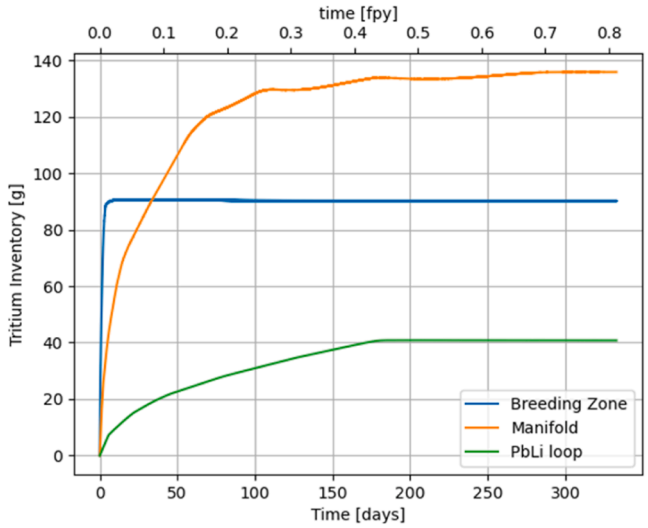


**Fig. 17.** Inventories of tritium trapped inside EUROFER.

### 3.4.1. *Magnetoconvective analyses of a slice equipped with helical DWTs*

Numerical analyses with ANSYS CFX have been performed to support and substantiate the adoption of a cooling scheme based on nested helical pipes for the WCLL BZ. The realized model represents the proposed pipe layout in one of the six subchannels composing a WCLL slice. Spatially varying volumetric heating is applied to the PbLi and Eurofer to represent the interaction with fusion neutrons, as well as the static heat load on the FW armour, that is cooled by water flowing in embedded square channels. Convective heat transfer toward the coolant is represented by boundary conditions derived from the analysis presented in [10]. An inclined magnetic field is imposed on the computational domain to represent the effect of both the toroidal and poloidal components present in the reactor. To limit the computational cost, magnetic field intensity, expressed through the Hartmann number ($Ha = B_0L(\sigma/\rho\nu)^{0.5}$), is scaled down whilst maintaining a representative force balance between buoyancy, inertial and electromagnetic forces by keeping constant the value of the interaction parameters, $Gr/Ha^2$ and $Gr/Ha^2Re$, following the approach outlined in [43,44]. As such, the governing parameters in our numerical model are $Ha = 250$ (cf. $Ha = 9 \times 10^3$ at nominal magnetic field intensity [44,45]), $Re = 47.85$, $Gr/Ha^2 = 7.76$, and $Gr/Ha^2Re = 0.162$.

Fig. 18 shows the velocity, electric potential, and temperature distribution in the frontal part of the WCLL BU channel, also known as "plenum". A circulation dominated by a large-scale vortex pair (Fig. 18a) is generated by the combination of intense non-uniform volumetric heating and complex pipe layout. Electric potential isosurfaces, as shown in Fig. 18b, are useful to show the 3D distribution of the vortices that tend to become aligned with the magnetic field direction to minimise Ohmic dissipation [43,46].

A hotspot is formed in the liquid metal close to the plenum top stiffening plate (Fig. 18c), but the PbLi/Eurofer interface and bulk Eurofer maximum temperature is limited to approximately 513 °C; comfortably below the upper threshold of the temperature window for

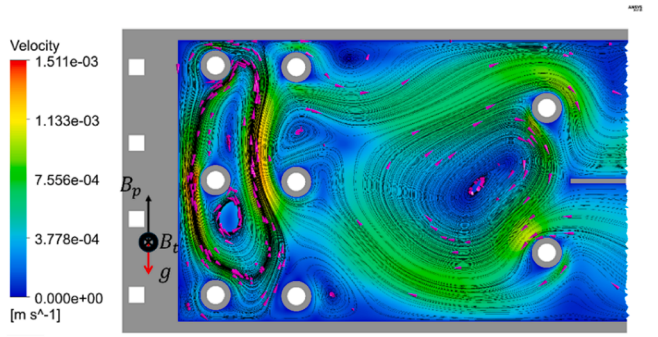


(a)

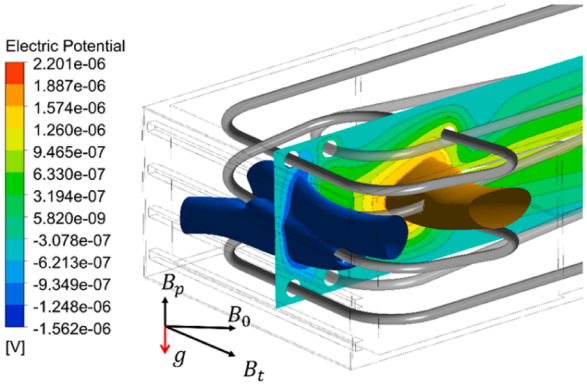


(b)

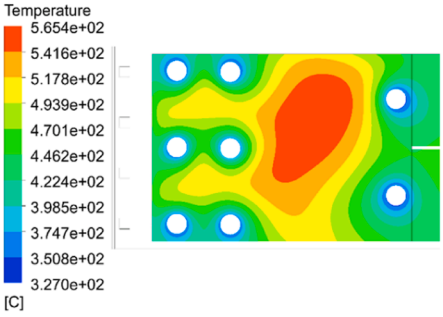


(c)

**Fig. 18.** Convective cells in the plenum region. (a) Velocity magnitude contour and streamlines plotted on the radial-poloidal midplane. (b) Electric potential contour on the radial-poloidal midplane and isopotential surfaces for $\varphi_1 = -1.15\times10–6$ V (blue) and $\varphi_2 = 1.6 \times 10–6$ V (orange) identifying the two principal circulation cells. (c) Temperature distribution in the liquid metal on the radial-poloidal plenum midplane.

the structural material [47], and slightly below the maximum temperature, 527 °C, reported by Maccari et al. for an analysis neglecting advective heat transfer [10]. More details about this study can be found in [45].

### 3.4.2. MHD flow in PbLi manifolds

MHD effects arise in the liquid metal breeder PbLi due to the interaction of flow-induced electric currents with the strong plasma-confining magnetic field. When duct walls are electrically conducting, currents may leak across common walls which results in an electrical coupling of neighbouring fluid domains [48,49], as for instance those in feeding and draining manifolds. Experimental and theoretical analyses for liquid metal blankets, in particular for test blanket modules (TBM) for ITER, show that the major fraction of pressure drop caused by MHD phenomena, arises in poloidal manifolds [50–53]. Here the velocity of PbLi is much higher than in breeder units (BUs) both due to the smaller cross-section and to the fact that one pair of manifolds has to supply the liquid metal flux to a large number N of BUs.

In the present study we consider poloidal manifolds like those suggested for the ITER TBM, which feature two parallel rectangular channels of different cross-section separated by a so-called baffle plate. A hybrid analysis method is applied, where the entire blanket module is split into typical sub-elements of poloidal length *dx*, which are stacked along the poloidal direction [54]. Feeding and draining manifold elements are electrically coupled via the common conducting baffle wall. The latter is located at non-dimensional position at $y = e$. MHD flows in such generic elements are determined by 3D simulations using asymptotic analysis valid for high Hartmann (Ha) numbers, and inertialess flow conditions. The Hartmann number serves as a nondimensional measure for the strength of the magnetic field and $Ha^2$ may be interpreted as the ratio of electromagnetic to viscous forces. One example of such simulations is displayed in Fig. 19, which shows velocity profiles in feeding and draining channels at two poloidal positions (a). The flows in the two ducts are driven in this example by the same poloidal pressure differences $\Delta p_d = \Delta p_f$. The manifold channels and baffle wall are penetrated near the local coordinate $x = 0$ by a stiffening plate [13]. The figure displays in addition in half of the geometry ($z \geq 0$) the distribution of electric potential on the fluid-wall interface (b).

From a number of such 3D simulations with different pressure heads in feeding and draining manifolds, $\Delta p_f \otimes \Delta p_d$, it is possible to derive a correlation that relates pressure drops $\Delta p_f$ and $\Delta p_d$ to flow rate fractions $\alpha_f$ and $\alpha_d$ in feeding and draining channels. The latter results are used in a global model that satisfies mass conservation

$$\alpha_f + \alpha_d = 1 \text{ and } \sum d\alpha_i = 1 \tag{2}$$

at each poloidal position, and for all BUs where $d\alpha_i$ denotes the fraction of flow through $BU_i$. For more details, see [54]. By considering the geometry of a TBM-like manifold, as shown in Fig. 20 (left), with the separating baffle wall at a constant position $e = 0.41$, the global distribution of flow rates in $N = 100$ BUs of DEMO blanket is plotted in Fig. 21 in blue. It can be seen that nearly all flow is exchanged via the first and last 10 BUs, while there is practically no flow through all remaining central BUs. It is obvious that such non-uniform flow partitioning is not acceptable for efficient tritium removal from the module. In order to resolve that deficit, an analysis has been performed for the determination of optimized positions $e_i$ of baffle walls [55], such that each BU receives same amount of flow (see black curve in Fig. 21). It is strongly recommended to update the manifold design and place the baffle wall to the optimized positions as displayed in Fig. 20 (right).

## 3.5. Structural performances

The verification of the structural performances of the BB under different loading scenarios is mandatory to demonstrate the soundness of its design. To this end, different analyses have been carried out in the past years [56,57]. Most of these studies have been focused on the behaviour of the FW and BZ neglecting the manifold area of the WCLL BB. To this purpose, RCC-MRx [58] rules against P-type damage have been checked to evaluate the performances of the assessed layouts. Moreover, these analyses have also highlighted the need of a revision of the BB attachment system to the VV to relieve the stress arising on these regions. The following sub-sections deal with these topics.

### 3.5.1. Parametric analysis and optimization of the revised manifold geometry

In the framework of the WCLL BB research activities, the COB equatorial elementary cell has been investigated from the structural point of view with the aim of evaluating its thermo-mechanical performances under selected loading conditions [59,60]. In particular, attention so far has been paid to the FW and BZ regions, without looking in detail at the performances of the manifold regions. Thus, the new manifold configuration of the COB equatorial cell has been investigated to assess its thermo-mechanical performances and to optimise the number and thickness of stiffening plates (SPs) in that region. A

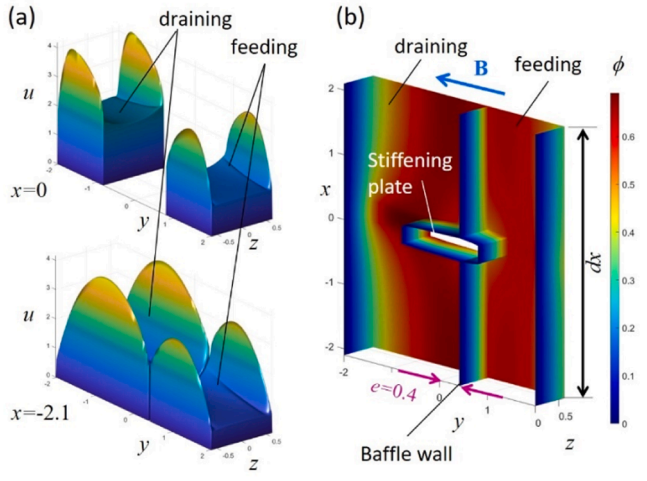


**Fig. 19.** MHD flow in a section dx of the poloidal manifolds. Velocity profiles (a) and electric potential φ (b) for Ha=1000 and $\Delta p_d = \Delta p_f$.

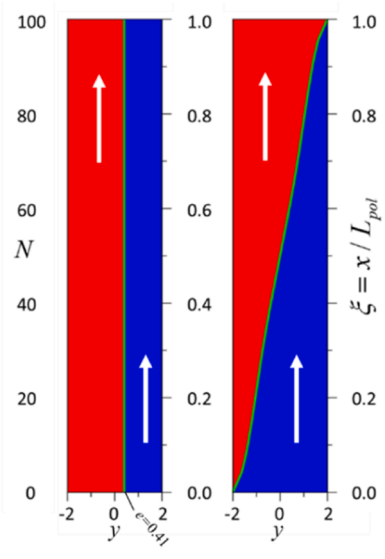


**Fig. 20.** Size of poloidal feeding (blue) and draining (red) manifolds for a TBM-like design (left) and for an optimized design for 100 BUs (right).

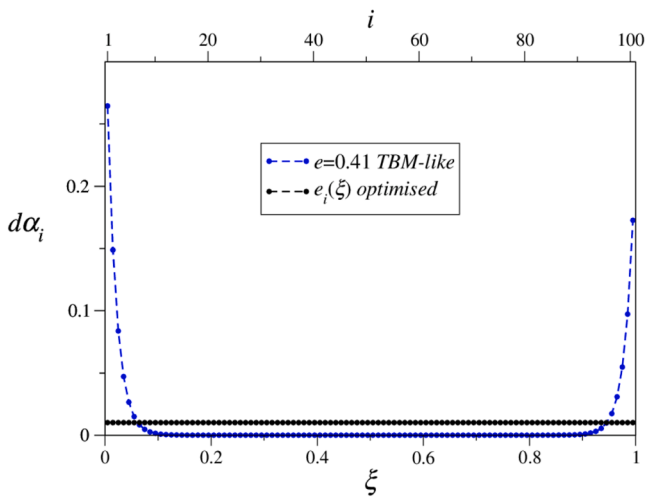


**Fig. 21.** Flow rate fractions $d\alpha_i$ in BUs along the scaled poloidal direction $\xi = x/L_{pol}$.

parametric analysis has been performed varying different geometric parameters. Firstly, the structural behaviour of three COB equatorial cells (Fig. 22) has been investigated considering only primary loads, i.e. internal pressure and mechanical restraints. Then, once a configuration able to withstand primary loads was obtained, the impact of the secondary loads has been evaluated.

The loads and boundary condition related to the Normal Operation (NO) loading scenario have been considered for the first phase of the activity. A pressure of 17.825 MPa (design value) has been imposed onto the water-wetted surfaces whereas a nominal pressure of 0.5 MPa has been considered for the breeder-wetted ones. As for the mechanical restraints, as reported in Fig. 22, in order to consider the presence of the entire segment, symmetry condition along the vertical direction and generalized plane strain have been imposed respectively onto the lower and upper surfaces. Moreover, the radial and toroidal displacements have been prevented to the nodes lying onto two lines obtained on the BSS external surface, to take into account the action of the attachment system.

Besides the initial configuration (called "v0"), the following configurations have been studied:

- v1: 4 poloidal-radial plates 3 mm-thick have been added in the water manifolds region;
- v2: the thickness of the 4 added plates has been increased to 5 mm;
- v3: the thickness of the 4 added plates has been increased up to the vertical SP one (12 mm);
- v4: the vertical SPs have been elongated up to the BSS.

Looking at the manifolds region of the central cell, a stress linearization procedure has been performed and some paths have been selected in those regions where the equivalent stress values overcome the maximum average allowable stress ($S_m$), and then their ratio exceeded the unit (Fig. 23). For the sake of brevity, only the results of the v4 configuration are reported (Table 6).

Globally, it can be observed that adding plates in the water manifolds region helps the structure to reduce the radial displacements and decreases the stress within both the PbLi and Water manifold regions.

Once a layout able to withstand the primary loads, fulfilling the corresponding RCC-MRx design criteria, has been obtained, the v4 configuration has been investigated under both NO (Level A) and the accidental (Level D) Over-Pressurization (OP) loading scenarios. Therefore, in addition to the NO scenario reported above, for the OP loading scenario a pressure of 17.825 MPa has been considered for both water and breeder-wetted surfaces. Moreover, a thermal field has been derived and properly adapted from a dedicated thermal-hydraulic analysis of the same equatorial region, missing of the water manifold region. Therefore, a uniform temperature of 311.5 °C has been applied onto this region. The same aforementioned mechanical restraints have been considered.

The "v4" layout shows good structural performances under both the NO and OP loading scenario. In fact, the selected RCC-MRx design criteria were fulfilled along all the considered paths, showing a good structural response of the model. Moreover, starting from "v4", the "v5" and "v6" configurations have been modelled by reducing the thickness of some plates in the water manifolds region (5 and 8.5 mm, respectively) and analyzed, with the aim of diminishing the total amount of steel in that region. Results show a worsening of the structural response just in the plates whose thickness has been decreased, no longer fulfilling the criteria of the standard. Therefore, the "v4" configuration has been considered as the reference one.

### 3.5.2. *Estimation of dynamic amplification factors*

During the functioning of a tokamak nuclear fusion reactor, plasma instabilities may take place, leading to a loss of confinement and the appearance of intense dynamic Electro-Magnetic (EM) loads [61]. In order to correctly take them into account and evaluate their impact on the BB structural behaviour, a simple static structural analysis may not be sufficient. Thus, the calculation of proper Dynamic Amplification Factors (DAFs) to envelope stresses caused by dynamic loads has been carried out.

To do so, a global model of the DEMO COB segment including the supports is developed. Two analyses (one static and one dynamic) were performed to calculate the DAFs. In both analyses and for each support, the reaction forces were computed and the support DAFs were calculated as the ratio between the max reaction force of dynamic analysis and the max reaction force of static analysis.

To model the behaviour of the supports (Fig. 24) proper boundary conditions and kinematic coupling conditions were adopted. In particular, a reference point for each support was created and its displacements along relevant directions were restrained. For each support, a spring was also used to consider the stiffness of the support. The implemented approach is a simplified practice and would consider a linear behaviour for the supports, so they have similar behaviour in

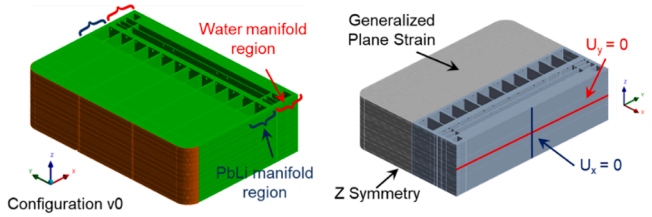


**Fig. 22.** Mechanical restraints.

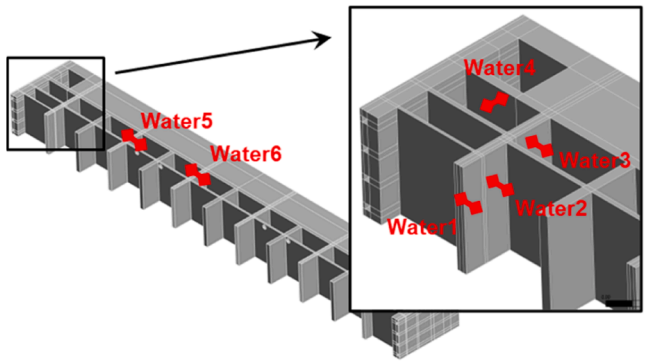


**Fig. 23.** Selected paths on the central cell manifold region.

**Table 6**
RCC-MRx criteria verification within v4 equatorial cell configuration.

| Path | 1 | 2 | 3 | 4 | 5 | 6 |
|---|---|---|---|---|---|---|
| $P_m/S_m$ | 0.80 | 0.77 | 0.79 | 0.60 | 0.82 | 0.82 |
| $(P_m+P_b)/(K_{eff}*S_m)$ | 0.59 | 0.62 | 0.62 | 0.63 | 0.56 | 0.55 |

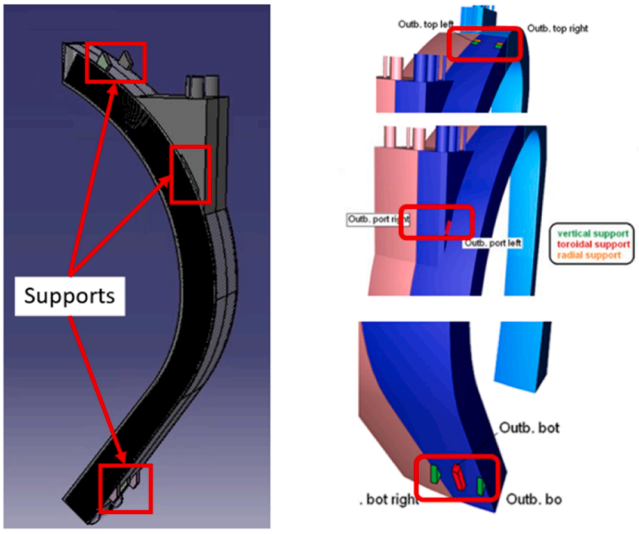


**Fig. 24.** The geometry of the blanket under study with location of the supports.

tension and compression.

The Vertical Displacement Event-UP (VDE-UP) in the time span of 10 s to 11.852 s has been considered as EM load for this study. Due to its characteristic and the purposes of the study, the blanket segment was modelled with shell elements, with a total number of nodes and elements equal to about 223k and 250k, respectively. As stated in advance, two analyses (one static and one dynamic) were performed to calculate the DAF. In both analyses and for each support, the reaction forces were extracted and the support DAFs were calculated. An example of the comparison of dynamic and static reaction forces is depicted in Fig. 25 for port left support. The peak responses are extracted and used for the calculation of DAF for all the supports and results are summarized in the Table 7. As it is observed the highest obtained DAF is equal to 2.6 which occurs in the case of port left support. Consequently, the suggested value for the final DAF to be considered on the COB segment supports is equal to 2.6.

As above said, the approach adopted in this study is a simplified practice considering a linear behaviour for the supports, so they have similar behaviour in both tension and compression modes. In future analysis more accurate modelling will be used to take into account the non-linear nature of the supports.

**Table 7**
List of calculated DAF for supports.

| Support name | Analysis | Max response [MN] | DAF |
|---|---|---|---|
| Top right radial & toroidal | Dynamic | 2.68 | 1.3 |
| | Static | 2.04 | |
| Top right vertical | Dynamic | 1.58 | 1.6 |
| | Static | 0.978 | |
| Top left radial & toroidal | Dynamic | 1.35 | 1.1 |
| | Static | 1.25 | |
| Top left vertical | Dynamic | 0.922 | 1.2 |
| | Static | 0.79 | |
| Port right | Dynamic | 0.625 | 2.3 |
| | Static | 0.270 | |
| Port left | Dynamic | 0.6 | 2.6 |
| | Static | 0.233 | |
| Bottom right radial | Dynamic | 1.85 | 1.1 |
| | Static | 1.68 | |
| Bottom right vertical | Dynamic | 1.75 | 1.0 |
| | Static | 1.73 | |
| Bottom left radial | Dynamic | 1.76 | 1.1 |
| | Static | 1.64 | |
| Bottom left vertical | Dynamic | 1.99 | 1.2 |
| | Static | 1.68 | |
| Bottom toroidal | Dynamic | 2.91 | 1.3 |
| | Static | 2.25 | |
| Max | – | – | 2.6 |

### 3.5.3. Revision of the attachment system

In order to evaluate the impact of a different BB attachment system to the VV, a simplified FE model of the Left OB segment (LOB) has been set up. The geometry has been simplified according to the main objectives of the analysis, meaning that the FW is modelled with an equivalent orthotropic shell section (approach validated for some representative mechanical and thermal scenarios) and the internals of the BZ are modelled by means of shell elements.

The simplified FE model has been used to perform thermo-mechanical analyses to study the structural integrity of the concept from a global point of view for two different BB-to-VV upper interface concepts (Fig. 26): Connecting Rod concept (CR-C) and Cylindrical Contact concept (CC-C) or vertically guided; and three equatorial plane interfaces: (i) no radial stopper, (ii) outward radial stopper and (iii) bidirectional radial stopper. Concerning the bottom part of the segment, the same solution relying on a spherical contact has been adopted for the two concepts.

The structural analysis performed consisted in the application of five sequential loading steps: (i) gravity (g); (ii) internal pressure P; (iii) thermal loads in two sub-steps, a uniform ramp-up from 40 °C to 300 °C ($T_0$) followed by the application of the (iv) temperature profiles during NO ($T_{NO}$); and (v) peak EM loads.

The global behaviour of the LOB is equivalent for both studied concepts. The main difference is that the CR-C imposes a paired radial-poloidal motion to the upper interface. Consequently, the CR-C moves radially outward more that the CC-C. In the following is reported the main effect of the different loads:

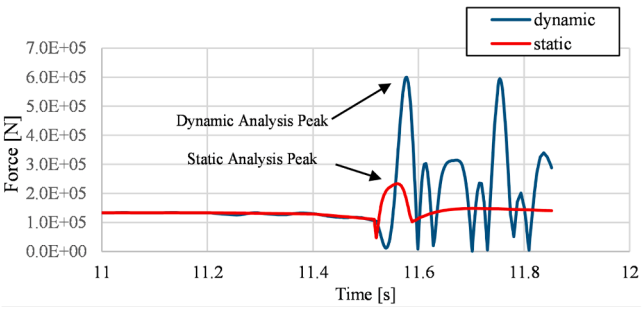


**Fig. 25.** Comparison of static and dynamic response for port left support.

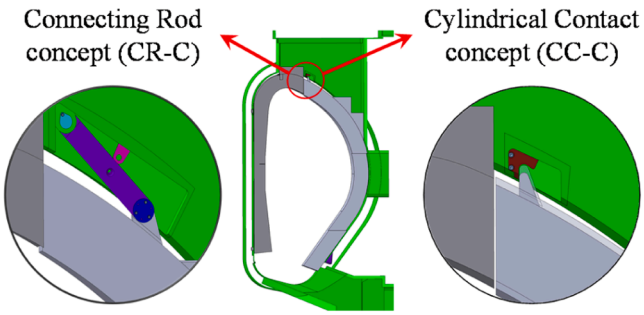


**Fig. 26.** The two proposed BB-to-VV attachment concepts.

i. g: does not represent significant load nor displacement.
ii. P: slightly opens the module.
iii. $T_0$: does not impose deformation, but a uniform expansion of the module. The module moves outwards at the equatorial plane.
iv. $T_{NO}$: opens the module, pushing the module inwards at the equatorial plane.
v. EM: induces a slight outward movement, but it is of a smaller value than that of $T_{NO}$.

Overall, stresses due to EM loads appear to be significantly smaller than those caused by thermal loads. Therefore, thermal loads are likely to be the main driver of the design, as reported in Fig. 27. Some areas have been identified to have large thermally induced stresses during $T_{NO}$, mainly the FW and the BP. These large stresses are related to the difference in temperature during NO conditions and the internal expansion restrictions imposed by the much more rigid and colder BSS.

The two proposed BB-to-VV mechanical interface concepts are demonstrated to be feasible based on the global structural checks performed on the LOB segment. However, the CR-Concept presents some advantages compared to the CC-C one. The main advantage is that it allows the free expansion of the module, thus minimising thermally induced stress. Additionally, the supporting conditions for the CR-C are constant over time as they do not rely on the closure of non-linear contacts, in contrast to those of the CC-C. The main concern of the CR-C is the relative motion between the BB and the VV as the module is free to expand (reach up to 100 mm at the upper interface).

The analyses performed suggest that the addition of a bidirectional radial stopper is not needed as the segment tends to move outward during the NO conditions. On the other hand, the outward radial stopper could be beneficial in the CR-C for two main reasons. The first reason would be the limitation of the outward movement of the segment with respect to the VV. The second, is that due to the deformation of the segment imposed by both the equatorial and upper (CR-C) interfaces, the stress values of the BP seem to decrease.

## 4. Conclusions and outlooks

Over the past years several modifications have been made to the WCLL BB architecture achieved in the pre-conceptual design phase [9], with the aim of overcoming the existing issues and improving its performances. In particular, the adoption of helical DWTs has allowed the improvement of several figures of merits to be reached, from both thermal, structural, tritium permeation and MHD point of views. Moreover, this new layout also increases the representativeness of the WCLL BB with respect to the ITER WCLL-TBM [13].

Nevertheless, different sensitivities are still on-going, with the twofold goal of further improving the WCLL BB performances to reach the values prescribed by the DEMO design team and providing a comprehensive set of documents in view of the next Gate Review foreseen during mid-2025.

Despite the significant steps forward made in the last years on the design point of view, at this stage it becomes of fundamental importance the experimental verification of some design solutions (e.g. the FW and manifold layouts), as well as the validation of the numerical codes adopted to perform the design and to predict some WCLL BB relevant phenomena, such as MHD in relevant geometries, PbLi-Water interaction and so on. To achieve this goal, it will be of pivotal importance the construction, commissioning and exercise of experimental infrastructures like W-HYDRA [62] and MaPLE [63].

## CRediT authorship contribution statement

**P. Arena:** Writing – review & editing, Writing – original draft, Supervision, Methodology, Conceptualization. **A. Del Nevo:** Supervision. **J. Aktaa:** Writing – review & editing. **G. Bongiovì:** Writing – original draft, Investigation. **L. Bühler:** Writing – original draft. **I. Catanzaro:** Writing – original draft, Software. **S. Cesaroni:** Software. **G. Caruso:** Supervision. **B. Chelihi:** Writing – original draft, Software. **C. Ciurluini:** Writing – original draft, Software. **A. Collaku:** Writing – original draft, Investigation. **F. Colliva:** Software. **C. Garnier:** Writing – original draft, Investigation. **F. Giannetti:** Supervision. **P. Haghdoust:** Writing – original draft, Investigation. **V. Imbriani:** Software. **F. Lucca:** Supervision. **P. Maccari:** Writing – original draft, Software. **L. Maqueda:** Supervision. **L. Melchiorri:** Writing – original draft, Software. **C. Mistrangelo:** Writing – original draft. **G. Mongiardini:** Writing – original draft, Software. **F. Moro:** Writing – original draft, Investigation. **T. Moulignier:** Supervision. **R. Mozzillo:** Supervision. **S. Noce:** Writing – original draft, Investigation. **I. Pagani:** Supervision, Software. **J.B. Pontier:** Supervision. **T. Pomella Lobo:** Writing – original draft, Supervision. **M. Principato:** Software. **P. Ruiz:** Writing – original draft, Software. **L. Savoldi:** Supervision. **S. Siriano:** Writing – original draft, Investigation. **A. Tassone:** Writing – review & editing, Supervision. **F.R. Urgorri:** Writing – original draft, Investigation. **F. Viganò:** Supervision. **Á. Yañez:** Writing – original draft, Software.

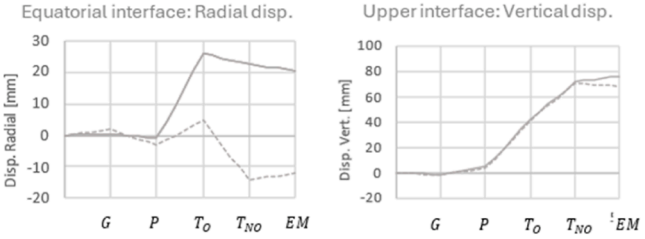


**Fig. 27.** Displacements calculated for the different steps.

## Declaration of competing interest

The authors declare that they have no known competing financial interests or personal relationships that could have appeared to influence the work reported in this paper.

## Acknowledgments

This work has been carried out within the framework of the EUROfusion Consortium, funded by the European Union via the Euratom Research and Training Programme (Grant Agreement No 101052200-EUROfusion). Views and opinions expressed are however those of the author(s) only and do not necessarily reflect those of the European Union or the European Commission. Neither the European Union nor the European Commission can be held responsible for them.

## Data availability

Data will be made available on request.

## References

[1] W. Morris, et al., European Research Roadmap to the Realisation of Fusion Energy, EUROFusion, Garching, Germany, 2018. ISBN 978-3-00-061152-0.
[2] A. Del Nevo, et al., Recent progress in developing a feasible and integrated conceptual design of the WCLL BB in EUROfusion project, Fusion Eng. Des. 146 (2019) 1805–1809.
[3] P. Arena, et al., The DEMO water-cooled lead–Lithium breeding blanket: design status at the end of the pre-conceptual design phase, Appl. Sci. 11 (2021) 11592.
[4] P. Arena, et al., Design and integration of the EU-DEMO water-cooled lead lithium breeding blanket, Energies. (Basel) 16 (2023) 2069.
[5] F.A. Hernández, et al., Consolidated design of the HCPB breeding blanket for the pre-conceptual design phase of the EU DEMO and harmonization with the ITER HCPB TBM program, Fusion Eng. Des. 157 (2020) 111614.
[6] G. Zhou, et al., The European DEMO helium cooled pebble bed breeding blanket: design status at the conclusion of the pre-concept design phase, Energies. (Basel) 16 (2023) 5377.
[7] P. Pereslavtsev, et al., Neutronic activity for development of the promising alternative water-cooled DEMO concepts, Appl. Sci. 13 (2023) 7383.

[8] S. Giambrone, et al., Preliminary thermo-mechanical assessment of the top cap region of the water-cooled lead-ceramic breeder breeding blanket alternative concept, Fusion Eng. Des. 200 (2024) 114201.
[9] L.V. Boccaccini, et al., Status of maturation of critical technologies and systems design: breeding blanket, Fusion Eng. Des. 179 (2022) 113116.
[10] P. Maccari, et al., Helical-shaped double wall tubes solution for the breeding zone cooling in the WCLL breeding blanket, Fusion Eng. Des. 199 (2024) 114134.
[11] G. Bongiovì, et al., Multi-module vs. single-module concept: comparison of thermomechanical performances for the DEMO water-cooled lithium lead breeding blanket, Fusion Eng. Des. 136 (2018) 1472–1478.
[12] U. Fischer, et al., Achievable and target TBR for the European DEMO, Fusion Eng. Des. 155 (2020) 111553.
[13] J. Aubert, et al., Design and preliminary analyses of the new water cooled lithium lead TBM for ITER, Fusion Eng. Des. 160 (2020) 111921.
[14] X-5 Monte Carlo Team, MCNP - a General Monte Carlo N-Particle Transport Code, Version 5, Los Alamos National Laboratory, Los Alamos, New Mexico, USA, 2003 April.
[15] JEFF3.3 nuclear data library (2025), http://www.oecd-nea.org/dbdata/jeff/jeff33/#neutron.
[16] F. Moro, et al., Neutronic analyses in support of the WCLL DEMO design development, Fusion Eng. Des. 136 (2018) 1260–1264.
[17] S. Noce, et al., Nuclear analysis of the single module segment WCLL DEMO, Fusion Eng. Des. 147 (2019) 111207.
[18] F. Moro, et al., Nuclear analysis of the water cooled lithium lead DEMO reactor, Fusion Eng. Des. 160 (2020) 111833.
[19] F. Moro, et al., Nuclear performances of the water-cooled lithium lead DEMO reactor: neutronic analysis on a fully heterogeneous model, Fusion Eng. Des. 168 (2021) 112514.
[20] C. Bachmann, et al., Overview over DEMO design integration challenges and their impact on component design concepts, Fusion Eng. Des. 136 (2018) 87–95.
[21] U. Fischer, et al., Neutronic analyses and tools development efforts in the European DEMO programme, Fusion Eng. Des. 89 (9–10) (2014) 1880–1884.
[22] U. Fischer, et al., Methodological approach for DEMO neutronics in the European PPPT programme: tools, data and analyses, Fusion Eng. Des. 123 (2017) 26–31.
[23] E. Martelli, et al., Advancements in DEMO WCLL breeding blanket design and integration, Int. J. Energy Res. 42 (1) (2018) 27–52.
[24] A. Tassone, et al., Recent progress in the WCLL breeding blanket design for the DEMO fusion reactor, IEEE Trans. Plasma Sci. 46 (5) (2018) 1446–1457.
[25] U. Fischer, et al., Neutronic performance issues of the breeding blanket options for the European DEMO fusion power plant, Fusion Eng. Des. 109-111 (2016) 1458–1463.
[26] F. Moro, et al., Nuclear analyses in support of the water-cooled lithium lead breeding blanket design development: a prospective strategy to achieve the tritium self-sufficiency, presented at the, in: Proceedings of the 33rd SOFT 2024, 22-27 September, Dublin, Ireland, 2024. submitted to Fusion Engineering and Design.
[27] F. Maviglia, et al., Impact of plasma-wall interaction and exhaust on the EU-DEMO design, Nucl. Mater. Energy 26 (2021) 100897.
[28] M. Principato, C. Ciurluini, F. Giannetti, A. Del Nevo, System code simulation of DEMO WCLL central outboard blanket equatorial cell operational transients, Fusion Eng. Des. 20 (2024) 114220.
[29] The US Nuclear Regulatory Commission (USNRC), RELAP5/MOD3.3 Code Manual Volume 1: Code Structure, System Models, and Solution Methods, NUREG/CR-5535 (1995).
[30] E. Martelli, et al., Thermal-hydraulic modeling and analyses of the water-cooled EU DEMO using RELAP5 system code, Fusion Eng. Des. 146 (2019) 1121–1125.
[31] F. Edemetti, et al., Optimization of the first wall cooling system for the DEMO WCLL blanket, Fusion Eng. Des. 161 (2020) 111903.
[32] F. Edemetti, et al., Thermal-hydraulic analysis of the DEMO WCLL elementary cell: BZ tubes layout optimization, Fusion Eng. Des. 160 (2020) 111956.
[33] F. Colliva, et al., On the evaluation of the DEMO WCLL breeding blanket sector thermal-hydraulic performances at a system level, Presented At the, in: Proceedings of the 33rd SOFT 2024, 2024, 22-27 SeptemberDublin, Ireland, submitted to Fusion Engineering and Design.
[34] A. Allio, et al., Hybrid modelling for the manifolds and coolant flow distribution in the water-cooled lead-lithium of the EU-DEMO reactor, in: Proceedings of the 19th International Topical Meeting on Nuclear Reactor Thermal Hydraulics (NURETH-19), Brussels, Belgium, 6–11 March, 2022.
[35] G.A. Spagnuolo, et al., Integration issues on tritium management of the European DEMO breeding blanket and ancillary systems, Fusion Eng. Des. 171 (2021) 112573.
[36] G.A. Spagnuolo, et al., Integrated design of breeding blanket and ancillary systems related to the use of helium or water as a coolant and impact on the overall plant design, Fusion Eng. Des. 173 (2021) 112933.
[37] F. Urgorri, et al., Preliminary system modeling for the EUROfusion water cooled lithium lead blanket, Fusion Sci. Technol. 71 (3) (2017) 444–449.
[38] F. Urgorri, et al., Tritium transport modeling at system level for the EUROfusion dual coolant lithium-lead breeding blanket, Nucl. Fusion 57 (11) (2017) 116045.
[39] F. Reiter, Solubility and diffusivity of hydrogen isotopes in liquid Pb-17Li, Fusion Eng. Des. 14 (1991) 207–211.
[40] G.A. Esteban, et al., Hydrogen transport and trapping in EUROFER'97, J. Nucl. Mater. 367-370 (2007) 473–477.
[41] I. Peñalva, et al., Experimental determination of the surface rate constants of protium and deuterium in Eurofer97, Nucl. Mater. Energy 38 (2024) 101618.
[42] F. Montupet-Leblond, et al., Permeation and trapping of hydrogen in Eurofer97, Nucl. Mater. Energy 29 (2021) 101062.
[43] F. Urgorri, et al., Magneto-convective analyses of the PbLi flow for the EU-WCLL fusion breeding blanket, Energies. (Basel) 14 (19) (2021) 6192.
[44] S. Siriano, et al., Numerical investigation of liquid metal convection at high Grashof and Hartmann number in a prototypical water-cooled breeding blanket for fusion reactors, Int. J. Heat. Mass Transf. 242 (2025) 126840.
[45] A. Tassone and S. Siriano, 2025 Magnetohydrodynamic simulation of the WCLL breeding blanket with helical cooling pipes. Available at SSRN, doi:10.2139/ssrn.5125573.
[46] U. Müller, L. Bühler. Magnetofluiddynamics in Channels and Containers, Springer, 2001.
[47] G. Van Oost, Fundamentals of Magnetic Fusion Technology, editor, IAEA, 2023.
[48] C. Mistrangelo, L. Bühler, Electro-magnetic flow coupling for liquid metal blanket applications, Fusion Eng. Des. 109-111 (2016) 1452–1457.
[49] C. Mistrangelo, L. Bühler, Determination of multichannel MHD velocity profiles from wall-potential measurements and numerical simulations, Fusion Eng. Des. 130 (2018) 137–141.
[50] L. Bühler, C. Mistrangelo, H.-J. Brinkmann, C. Koehly, Pressure distribution in MHD flows in an experimental test-section for a HCLL blanket, Fusion Eng. Des. 127 (2018) 168–172.
[51] C. Courtessole, H.-J. Brinkmann, L. Bühler, J. Roth, Experimental investigation of MHD flows in a WCLL TBM mock-up, Fusion Eng. Des. 202 (2024) 114306.
[52] L. Bühler, C. Courtessole, B. Lyu, C. Mistrangelo, Electric potential on a WCLL TBM mock-up in MHD experiments as indication for flow distribution in breeder units, Fusion Eng. Des. 212 (2025) 114846.
[53] C. Courtessole, H.-J. Brinkmann, L. Bühler, J. Roth, Characterization of MHD pressure losses in a mock-up of the WCLL test blanket module, presented at the, in: Proceedings of the 33rd SOFT 2024, 22-27 September, Dublin, Ireland, 2024. submitted to Fusion Engineering and Design.
[54] L. Bühler, C. Mistrangelo, A simple MHD model for coupling poloidal manifolds to breeder units in liquid metal blankets, Fusion Eng. Des. 191 (2023) 113552.
[55] L. Bühler, C. Mistrangelo, Geometric optimization of electrically coupled liquid metal manifolds for WCLL blankets, IEEE Trans. Plasma Sci. 202 (2024) 114306.
[56] I. Catanzaro, et al., Structural assessment of the EU-DEMO water-cooled lead lithium central outboard blanket segment adopting the sub-modelling technique, Fusion Eng. Des. 192 (2023) 113601.
[57] S. Giambrone, et al., Study of the thermo-mechanical performances of the EU-DEMO water-cooled lead lithium left outboard blanket segment, Fusion Eng. Des. 192 (2023) 113837.
[58] AFCEN, RCC-MRx, Design and Construction Rules For Mechanical Components of Nuclear Installations, Courbevoie, 2013. France.
[59] J.A. Noguerón, et al., Numerical investigation of the structural performances of the EU-DEMO water-cooled lead lithium breeding blanket equipped with helicoidal double-walled tubes, Fusion Eng. Des. 208 (2024) 114703.
[60] I. Catanzaro, et al., Development and application of an alternative modelling approach for the thermo-mechanical analysis of a DEMO water-cooled lithium lead breeding blanket segment, Fusion Eng. Des. 180 (2022) 113195.
[61] I.A. Maione, et al., Electromagnetic analysis activities in support of the breeding blanket during the DEMO pre-conceptual design phase: methodology and main results, Fusion Eng. Des. 166 (2021) 112285.
[62] P. Arena, et al., W-HYDRA: a new experimental platform for the water-cooled lead lithium breeding blanket, Nucl. Fusion 64 (2024) 076043.
[63] L. Bühler, et al., Liquid metal MHD research at KIT: fundamental phenomena and flows in complex blanket geometries, Fusion Eng. Des. 200 (2024) 114195.